FISEVIER

Contents lists available at ScienceDirect

### **International Journal of Plasticity**

journal homepage: www.elsevier.com/locate/ijplas



## Portevin-Le Chatelier mechanism in face-centered-cubic metallic alloys from low to high entropy



Che-Wei Tsai<sup>a,b</sup>, Chi Lee<sup>a</sup>, Po-Ting Lin<sup>a,b</sup>, Xie Xie<sup>c</sup>, Shuying Chen<sup>c</sup>, Robert Carroll<sup>d</sup>, Michael LeBlanc<sup>d</sup>, Braden A.W. Brinkman<sup>e</sup>, Peter K. Liaw<sup>b,c,\*\*</sup>, Karin A. Dahmen<sup>d,\*\*\*</sup>, Jien-Wei Yeh<sup>a,b,\*</sup>

- <sup>a</sup> Department of Materials Science and Engineering, National Tsing Hua University, Hsinchu, 30013, Taiwan
- <sup>b</sup> High Entropy Materials Center, National Tsing Hua University, Hsinchu, 30013, Taiwan
- <sup>c</sup> Department of Materials Science and Engineering, The University of Tennessee-Knoxville, Knoxville, TN, 37996, USA
- d Department of Physics, University of Illinois at Urbana-Champaign, 1110 West Green Street, Urbana, IL, 61801, USA
- <sup>e</sup> Department of Applied Mathematics, University of Washington, Seattle, WA, 98195, USA

#### ARTICLE INFO

# Keywords: Portevin-Le Chatelier effect Serration mechanism Medium-entropy alloy High-entropy alloy

Substitutional alloy

#### ABSTRACT

Serration phenomena during tensile testing on certain alloys with diffusing solute atoms (i.e., Portevin–Le Chatelier effect) have been observed for a long time, but detailed mechanisms are not fully clear yet. This study is intended to find the mechanism from different approaches verified by tensile testing on a series of single-phase face-centered-cubic (FCC) pure metal and alloys: Ni, CoNi, CoFeNi, CoCrFeNi, and CoCrFeMnNi, which range from low to high configurational entropy. The results of tensile tests, at strain rates from  $1\times10^{-5}$  to  $1\times10^{-2}/s$  and temperature from room temperature to 700 °C, show that serrations occur on stress-strain curves of CoFeNi, CoCrFeNi, and CoCrFeMnNi alloys in their specific temperature and strain-rate regime. A mechanism for dislocation pinning is proposed and verified with theoretical calculation for the present substitutional alloys. The proposed mechanism involves the in-situ rearrangement of substitutional solute atoms by "local dislocation-core diffusion" and might also be applied to similar substitutional alloys.

#### 1. Introduction

High-entropy alloys (HEAs) are potentially promising for structural applications (Cantor et al., 2004; Chuang et al., 2011; Hemphill et al., 2012; Miracle and Senkov, 2017; Otto et al., 2013; Senkov et al., 2010; Tong et al., 2005; Yeh, 2006, 2013; Yeh et al., 2004, 2007; Youssef et al., 2015; Zhang et al., 2013, 2014). They could exhibit good high-temperature softening resistance (Chuang et al., 2011; Tong et al., 2005), high ductility (Hemphill et al., 2012; Li et al., 2016; Otto et al., 2013; Tong et al., 2005), good fatigue resistance (Hemphill et al., 2012; Tang et al., 2015), as well as outstanding wear resistance (Chuang et al., 2011; Tong et al., 2005). HEAs are defined as having a mixing entropy greater than 1.5R in their random solution state, where R is the gas constant. Moreover, medium-entropy alloys (MEAs) and low-entropy alloys (LEAs) are defined as those having the mixing entropy between 1R and 1.5R, and those below 1R, respectively (Yeh, 2013).

E-mail addresses: pliaw@utk.edu (P.K. Liaw), dahmen@illinois.edu (K.A. Dahmen),

<sup>\*</sup> Corresponding author. Department of Materials Science and Engineering, National Tsing Hua University, Hsinchu, 30013, Taiwan.

<sup>\*\*</sup> Corresponding author. High Entropy Materials Center, National Tsing Hua University, Hsinchu, 30013, Taiwan.

<sup>\*\*\*</sup> Corresponding author.

Serration behavior of metallic materials has long been an important issue for materials scientists (Halim et al., 2007; Hector and Zavattieri, 2011; Rizzi and Hahner, 2004; Zavattieri et al., 2009). As a result, the serration behavior of HEAs in mechanical testing have also been reported as HEAs attract researchers' attention. For example, Tong et al. investigated mechanical properties of  $Al_x$ CoCrCuFeNi alloys (x = 0.5, 1.0, and 2.0) and showed the first observation of serration phenomena in the compression curves of  $Al_{0.5}$ CoCrCuFeNi at 300 °C and 500 °C when the strain rate was  $1 \times 10^{-3}$ /s (Tong et al., 2005). Otto et al. studied the tensile properties and micro-structural evolution during deformation of the solo face-centered-cubic CoCrFeMnNi equi-atomic alloy (Otto et al., 2013). Pronounced serration behaviors in tensile stress-stain curves were also observed at 400 °C and the strain rate of  $1 \times 10^{-3}$ /s. However, the serrations in the stress-strain curves had not yet been investigated and explained (Antonaglia et al., 2014; Otto et al., 2013). For this reason, our research group had made a systematic study on this behavior in order to find the relevant serration mechanism (Portevin-Le Chatelier effect, abbreviated as PLC effect) for substitutional alloys and reported the results and statistical analyses (Carroll et al., 2015). In the research, we prepared a series of FCC metal and alloys: Ni (LEA), CoNi (LEA), CoFeNi (MEA), CoCrFeNi (MEA), and CoCrFeMnNi (HEA) and performed tensile testing at different temperatures from 300 to 700 °C and strain rates from  $1 \times 10^{-5}$  to  $1 \times 10^{-2}$ /s. Since they all have a solo FCC structure, they could provide a common basis for comparing serration behaviors. Their configurational entropies are 0R, 0.69R, 1.1R, 1.39R, and 1.61R, respectively. Thus, the alloy series covers LEAs, MEAs, and HEAs, providing a broad range in the matrix composition. This feature becomes helpful to clarify the effects of adding substitutional elements, temperatures (from 300 °C to 700 °C), and strain rates (from  $1 \times 10^{-5}$  to  $1 \times 10^{-2}$ /s) (Carroll et al., 2015) on the serration characteristics.

From the previous results of tensile testing, the PLC effect had been found in a specific range of temperatures and strain rates for MEAs and HEAs, but not for LEAs representing the conventional substitutional alloys (Carroll et al., 2015). This trend indicates that stress drops or "serrations" only occur in a particular range of temperatures depending on the composition and strain rate, which is a phenomenon reported in other conventional alloys as well (Min et al., 2016). Knowledge of this special characteristic is important for applications of alloys, and therefore we made a study of serration mechanisms for substitutional alloys. It was found that the serration statistics with temperatures and strain rates are in excellent agreement with the predictions of our mean-field theory (MFT) model (Carroll et al., 2015). The serration behavior indicates that dislocations, also referred to as weak spots in the model (Carroll et al., 2015), which move along slip planes (when a sufficiently-large shear stress is applied) trigger other dislocations to slip, giving in slip avalanches generally detected as sudden stress drops. During slip avalanches, the involved weak spots are weakened from their original strength to a lower strength, but they are re-strengthened during the time intervals between slip avalanches. Re-strengthening or healing of weak spots between slip avalanches is temperature-, strain-rate- and composition-dependent. More abundant sources of solute atoms result in greater healing rates. The healing rate approaches a maximum at a material-specific temperature and strain rate.

Our previous work was followed by a few research discussing the serration behavior of HEAs (Fu et al., 2017; Wang et al., 2017; Zhang et al., 2016). Wang et al. proposed a cluster + glue-atom model and studied the atomic and electronic basis for the valence-electron-concentration-categorized principles and the observed serration behavior in refractory MEAs, MoNbTaW, MoNbVW, MoTaVW, HfNbTiZr, and metallic glass  $Zr_{41}Ti_{14}Cu_{12.5}Ni_{10}Be_{22.5}$ . They found that the presence of strongly bonded clusters and weakly bonded glue atoms implies a serrated deformation of the alloys, resulting in intermittent avalanches of defect movement (Wang et al., 2017). On the other hand, Fu et al. studied the tensile properties and serrated flow behavior of CoCrFeNiMn HEA and found the similar serration behavior as in our previous observation. They further derived two activation energies for serrated flow over different temperature ranges and concluded that the activation energy of 116 kJ mol<sup>-1</sup> in the range of 300–500 °C implied that pipe diffusion is responsible for the pinning process of dislocations. In contrast, a higher activation energy of 295 kJ mol<sup>-1</sup> calculated between 500 and 600 °C suggested that the pinning or unpinning process of dislocations is controlled by Ni atoms, the constituent element with the highest activation energy for lattice diffusion in the CoCrFeMnNi HEA (Fu et al., 2017; Tsai et al., 2013). However, the actual process in which solute atoms diffuse and then pin the dislocation in the short time scale during serration is still unclear.

In the present study, aside from the MFT model and mechanisms that we discussed in the previous literature, we further consider the conventional mechanisms for serration phenomena and the multi-element diffusion of substitutional solute atoms in MEAs and HEAs. Finally, we propose a microscopic deformation mechanisms to explain the serration effect in MEAs, HEAs, and other substitutional alloys, and summarize the key features of the proposed mechanisms.

#### 2. Material and methods

In our research, a series of equiatomic materials containing Ni–Ni, CoNi, CoFeNi, CoCrFeNi, and CoCrFeMnNi were designed. They were vacuum arc-melted and solidified in a water-cooled copper crucible under the protection of argon from the elemental materials higher than 99.9 wt percent (wt.%) in purity. To assure the uniform composition, each specimen was repetitively melted and solidified at least four times. The samples obtained were slabs with dimensions,  $10 \text{ mm} \times 20 \text{ mm} \times 40 \text{ mm}$ . After machining the surface layer, each slab was cold-rolled with a 60% reduction in thickness, from 8 mm to 3.2 mm. The sheets were then homogenized at  $1100 \,^{\circ}\text{C}$  for 6 h and, subsequently, quenched in water. They were wire-cut into tensile specimens with dimensions shown in Fig. 1, on an electrical discharge machine. In order to prevent the influence of the contaminated surface layer, the specimen thickness is 1 mm. The tensile tests were performed on an Instron 4505 testing machine. Each of the five alloys was tested at room temperature (RT),  $300 \,^{\circ}\text{C}$ ,  $400 \,^{\circ}\text{C}$ ,  $500 \,^{\circ}\text{C}$ , and  $700 \,^{\circ}\text{C}$ , and with a strain rate of  $10^{-4}$ /s, equivalent to  $0.114 \, \text{mm/min}$  of displacement rate. The data-acquisition frequency of the tensile tests is  $20 \, \text{Hz}$ . The elastic strain is acquired using an extensometer, and the plastic strain is acquired by the testing machine. Moreover, the CoCrFeMnNi alloy samples were studied at  $275 \,^{\circ}\text{C}$ ,  $325 \,^{\circ}\text{C}$ ,  $375 \,^{\circ}\text{C}$ ,  $620 \,^{\circ}\text{C}$ , and  $650 \,^{\circ}\text{C}$ , with strain rates of  $10^{-2}$ /s, and  $10^{-5}$ /s, equivalent to  $11.4 \,^{\circ}\text{L}$ , and  $0.0114 \,^{\circ}\text{L}$  mm/min of displacement rate,

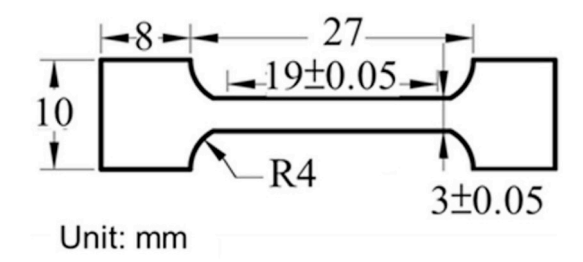


Fig. 1. Dimensions of the tensile samples employed in all tests.

respectively. Lastly, all stress-strain curves of the testing results are displayed as engineering stress-strain relations.

#### 3. Results

Stress-strain curves obtained from tensile testing at a strain rate of  $10^{-4}$ /s on (a) Ni, (b) CoNi, (c) CoFeNi, and (d) CoCrFeNi at RT, 300, 400, 500, 600, and 700 °C; (e) CoCrFeNiMn at 300, 400, 500, 600, 620, 650, and 700 °C; and (f) CoCrFeMnNi at 275, 300, 325, 350, 375, and 400 °C are shown in Fig. 2. It can be seen that all five single-phase FCC pure metal and alloys display ductile behavior with good elongations between 15% and 40% in the range of test temperatures and strain rates. It is also noted that the features of serrations are different but can be classified into three types: A, B, and C (Rodriguez, 1984). The identification of serration type is according to the classification adopted in the literature (Rodriguez, 1984; Zhang et al., 2017). Among these five types, Types A, B, and C are well-known and well documented. Type-A serrations feature a longer period of serrations, showing an abrupt and periodic rise in stress, followed by a drop to a stress value below the general level at certain points. They generally occur in the low temperature/high strain rate region of the dynamic strain aging (DSA) regime. Type-B serrations are oscillations about the general level of the stress-strain curve that occur in quick succession (i.e., shorter period). They occur at higher temperatures and lower strain rates of the DSA regime compared to Type A, and can also be developed from Type-A serrations with increasing strain. Type-C serrations are stress drops below the general level of the flow curve. They normally occur at higher temperatures and lower strain rates than Types A and B. Fig. 3 shows the examples of stress-strain curves characteristic of Types A, B, and C. Based on the above definitions of serrations, 14 samples display serration phenomena in which PLC bands display Type-A, B, or C characteristic among the 31 analyzed samples at different temperatures except RT, which can be seen elsewhere (Carroll et al., 2015).

At the strain rate of  $1 \times 10^{-4}$ /s, both the Ni metal and CoNi alloy do not exhibit serration behavior from RT to 700 °C. The CoFeNi, CoCrFeNi, and CoCrFeMnNi alloys have serrations from 400 °C to 500 °C, from 300 °C to 600 °C, and from 300 °C to 620 °C, respectively. It has been found that serrations occur from the ternary alloy to the quinary one. Furthermore, the temperature range of serrations broadens as the number of elements increases. However, the details of serration differ between quaternary and quinary alloys in the stress versus time curves, although these two alloys show serrated flow in similar temperature ranges. As for the evolution of serration type, the quinary alloy displays three different types evolving from Type A at low temperatures to Type B at medium temperatures and to Type C at high temperatures, which is consistent with the general findings from conventional alloys as mentioned in the last paragraph (Zhang et al., 2017). It is noted that even for Types A and B, the detailed features, i.e., the pitch and amplitude in the serrated curves, are still different in various alloys. Even in the same serrated curve, the detailed feature of the serration also differs at different strain values. All these feature differences are believed to be related to the non-uniform solute-dislocation and dislocation-dislocation interactions during the plastic flow (Rodriguez, 1984; Lebyodkin et al., 2012).

Fig. 4 shows the stress-strain curves obtained from tensile testing on CoCrFeMnNi at different strain rates for temperatures (a) 275 °C, (b) 300 °C, (c) 400 °C, (d) 500 °C, and (e) 600 °C. Fig. 5 is the summary of the temperature and strain rate range for the occurrence of the PLC effect in the CoCrFeMnNi alloy. It is noted that with increasing strain rate, there is a trend of serration types changing from Types C to B, to A, and to none. For examples, the combination of  $1 \times 10^{-2}$ /s and 300 °C gives no PLC effect. That of  $1 \times 10^{-4}$ /s and 275 °C exhibits no PLC effect but that of  $1 \times 10^{-5}$ /s and 275 °C presents PLC effects with Type B. This trend is similar to that with decreasing temperature, indicating that the PLC effect is still related to thermal-activation processes (Zhang et al., 2017).

From the above results, Ni and CoNi (LEA) possess no serration phenomena, but CoFeNi (MEA), CoCrFeNi (MEA), and CoCrFeMnNi (HEA) show serration features in a certain temperature range. Apparently, CoCrFeMnNi exhibits serration behavior in a temperature range similar to that of CoCrFeNi but broader than that of CoFeNi. This trend indicates that the structure of CoCrFeMnNi can allow atoms to pin the dislocations at lower temperatures and resist the larger thermal vibration to destroy the pinning influence. This trend seems unexpected, because serration phenomena could occur in such equiatomic alloys with substitutional solid solutions. Moreover, the quinary alloys presents the most pronounced PLC effect even though it has the slowest diffusion rate of atoms because of the sluggish diffusion effect (Tsai et al., 2013). Fig. 5 summarizes the conditions for the PLC effect in the CoCrFeMnNi alloy. It is noted that the PLC effect of CoCrFeMnNi continues at greater strain rates up to  $1 \times 10^{-2}$ /s for higher temperatures, except for the tests at 300 °C. This trend indicates that the pinning of dislocations is fast enough in CoCrFeMnNi alloy to show serrated flow under relatively high strain rate. Below we suggest a new pinning mechanism that explains the observations.

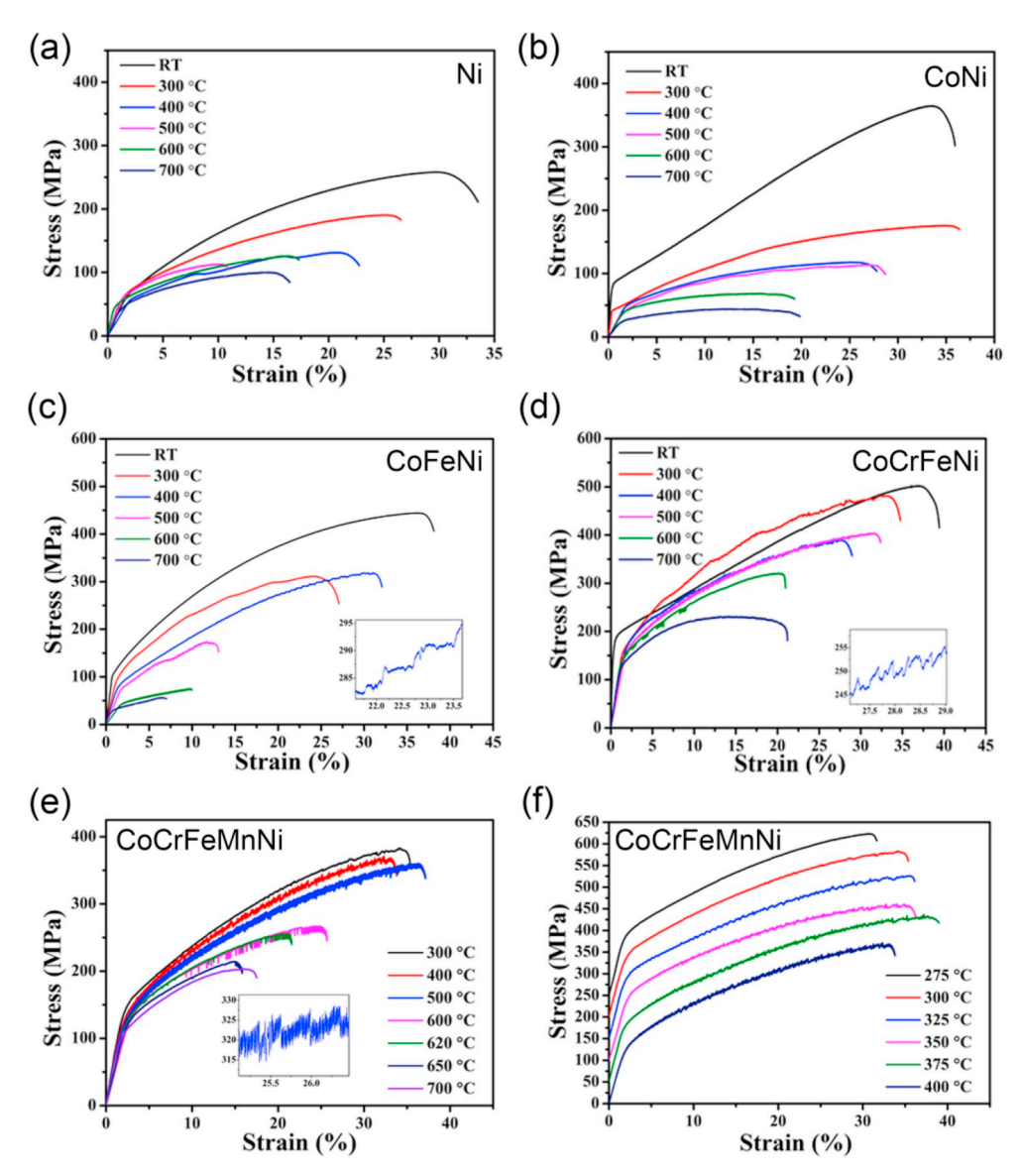


**Fig. 2.** Stress-strain curves obtained from tensile testing the strain rate of  $10^{-4}$ /s on (a) Ni, (b) CoNi, (c) CoFeNi, and (d) CoCrFeNi at RT, 300, 400, 500, 600, and 700 °C; (e) CoCrFeMnNi at 300, 400, 500, 600, 620, 650, and 700 °C; and (f) CoCrFeMnNi at 275, 300, 325, 350, 375, and 400 °C.

#### 4. Discussion

#### 4.1. Traditional mechanisms for the PLC effect

While the PLC effect is typically observed in certain conventional alloys (Kok et al., 2003; Rodriguez, 1984; Xiang et al., 2006; Yilmaz, 2011; Zhang et al., 2017), here we observe the PLC behavior in a limited temperature and strain-rate range for the present MEAs and HEAs. Traditionally, the quoted reason for the PLC effect is that solute atoms are able to pin the moving dislocations. There are two main mechanisms for interstitial alloys. One was originally proposed by Cottrell (Cottrell and Jaswon, 1949), by which the PLC effect occurs with the fast long-range diffusion of interstitials, i.e., the diffusion of interstitial atoms, such as C and N, at a rate faster than the speed of the dislocations so as to catch and lock them as the Cottrell atmosphere. As a result, dislocations have a drag force exerted by the atmosphere, and the stress must be increased for dislocations to break away from the solute pinning for the subsequent motion, thus causing a local stress increase and drop (Cottrell and Jaswon, 1949). However, a more acceptable dislocation arrest model was proposed by Sleeswyk (McCormic.Pg, 1973; Pink and Kumar, 1995; Sleeswyk, 1958). This model suggests that solute atmospheres form on forest dislocations and, then, drain by pipe diffusion from forest to mobile dislocations during their temporary arrest, when encountering forest dislocations. The waiting time, which is defined as the time period when mobile dislocations are temporarily arrested by forest dislocations, depends on temperatures, strain rates, stresses, and strains, since thermal

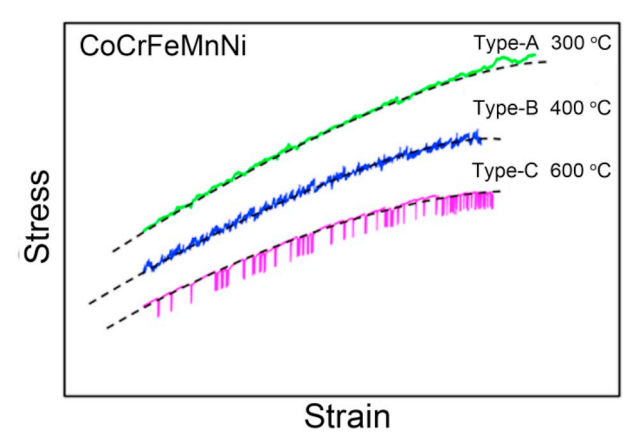


Fig. 3. Close-ups of experimentally measured stress versus strain curves. (a) Type-A example from CoCrFeMnNi, 300 °C at the strain rate of  $10^{-4}$ /s. (b) Type-B example from CoCrFeMnNi, 600 °C at the strain rate of  $10^{-4}$ /s.

activation and stress are needed to overcome the barriers. Two similar mechanisms for substitutional alloys have been proposed but with some differences. The first mechanism is also based on the Cottrell model but the diffusion of substitutional solute atoms must be accelerated by excess vacancies produced by quenching and deformation (Cottrell, 1953). The other mechanism is based on the dislocation-arrest model, originally proposed by Sleeswyk (1958) but replaces interstitial atoms by substitutional atoms (Mulford and Kocks, 1979; van den Beukel, 1975; van den Brink et al., 1975). As a result, for the alloys containing substitutional atoms and interstitial atoms, PLC effects are often explained using the pipe diffusion of both kinds of solute atoms. For example, C and Cr in the 316L stainless steel are responsible for these phenomena (Hong and Lee, 2005).

Therefore, the ratio of the strain rate to the temperature-dependent diffusion rate of solute atoms determines how much time the solute atoms need to attach to the dislocations prior to the increasing driving stress breaking the dislocations free from the cloud of diffusing atoms.

#### 4.2. Contradictions to traditional mechanisms

However, the traditional PLC mechanism by the simple diffusion of solute atoms through lattice or dislocation pipes cannot explain the observations in the present alloy series. We will check this with all traditional mechanisms including the early Cottrell model which has been early understood to be unrealistic. For example, in our alloys, we find that the temperature range for the PLC effect shifts downward and broadens with increasing number of elements. The temperature range having the PLC effects for the CoCrFeMnNi alloy is from 300 °C to 620 °C. Now, let's check the possible contributions of interstitial and substitutional atoms. Firstly, the trend of the temperature range for the PLC effect cannot be explained by interstitial atoms, since the present alloys contain less than several tens ppm of interstitial solute atoms of C, N, and O. The PLC effect in the soft iron was observed at 100 and 200 °C and disappeared at RT and 300 °C (Dieter, 1988). In plain-carbon steels, it occurs in the temperature range of 227–377 °C (Cottrell, 1953; Dieter, 1988; Pink and Kumar, 1995). Furthermore, it is well known that both interstitial and substitutional diffusion activities are less active in an FCC lattice than a BCC lattice. For example, considering the diffusion of carbon in iron at 910 °C, the intrinsic diffusion coefficient is about 100 times higher in the BCC iron than that in the FCC iron (Buffington et al., 1961; Porter and Easterling, 1981). Thus, it is almost impossible for the present FCC alloy series to have the interstitial atoms to catch moving dislocations and cause the PLC effect in the temperature range of 300 °C–620 °C.

Similarly, the observed PLC effects in this study cannot be explained by the simple diffusion of substitutional atoms in the lattice, because the diffusion rates of substitutional atoms are extremely low in the temperature range of 300 °C–620 °C in the present FCC alloys. They are even lower in alloys with a higher number of elements because of the sluggish diffusion effect (Tsai et al., 2013). This trend contradicts with the observation that the temperature range for the PLC effect shifts downward with the increasing number of elements, and the PLC effect is more pronounced in the present MEAs and HEAs than LEAs. Similar contradictions exist when considering the dislocation-arrest model (Cottrell and Jaswon, 1949; Xiang et al., 2006; Yilmaz, 2011) mentioned above. In the dislocation-arrest model, pipe diffusion along dislocation lines helps increase the diffusion rate of the solutes so that solute atoms can move from solute atmospheres formed on forest dislocations to temporarily arrested mobile dislocations and hinder their advancement. However, this model itself has some flaws which undermine the possibility of the above mechanism. The first is the assumption that forest dislocations are stationary and have atmospheres. This is unreasonable since the formation of atmospheres requires the long-range lattice diffusion of substitutional atoms from nearby regions (Rodriguez, 1984), which is extremely low during the total period spent in the tensile tests. The second is the drain of solute atoms from the cores of forest dislocations to arrested mobile dislocations. This process would not be energy effective given the fact that solutes are already at low energy sites, and only little energy could be released when the solutes move from forest dislocations to temporarily arrested mobile dislocations. That means the conventional drain mechanism could be more suitable for the dilute alloys which have been annealed to let solute

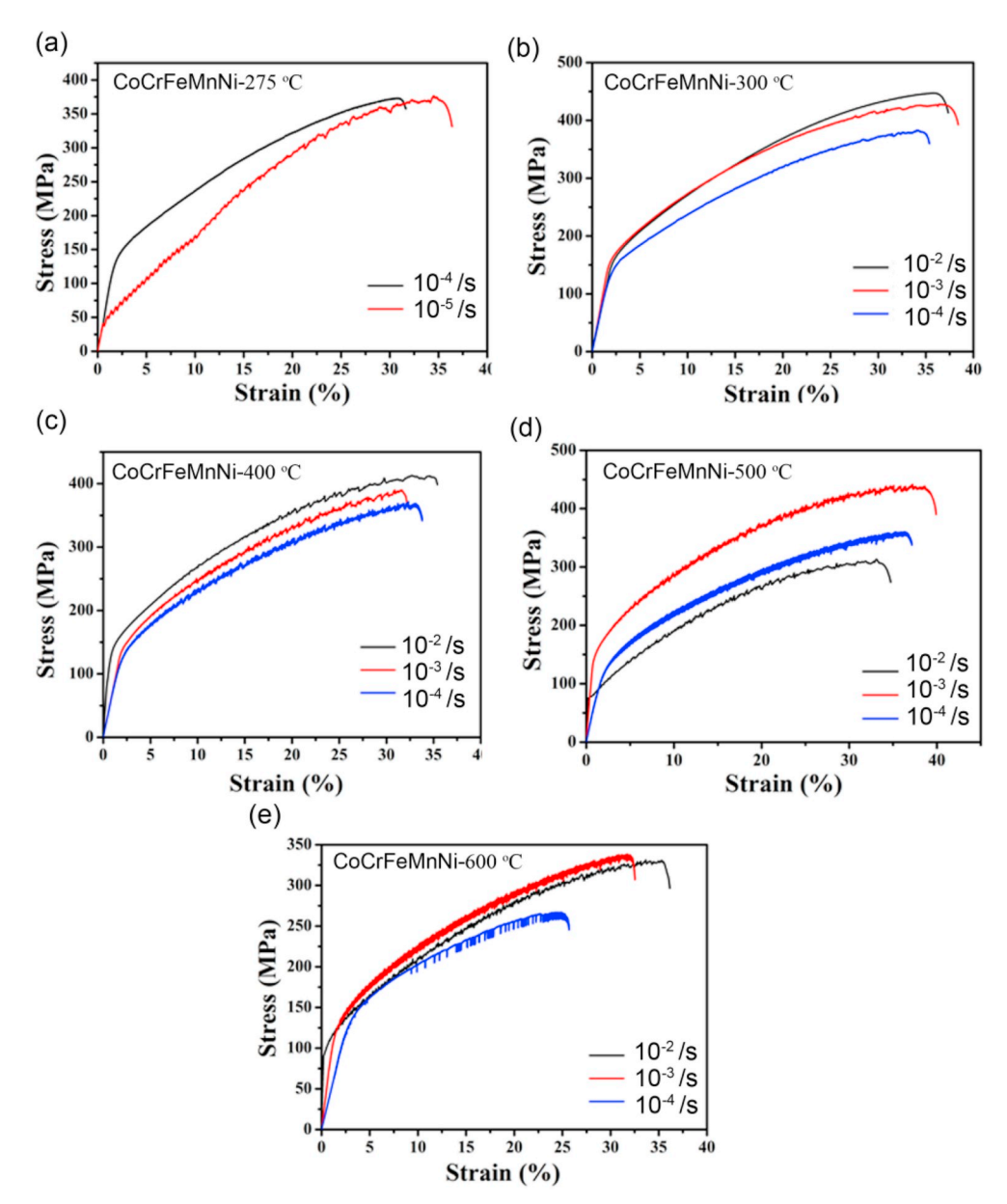


Fig. 4. Stress-strain curves obtained from tensile experiments on CoCrFeMnNi at different temperatures and strain rates (a) 275 °C, (b) 300 °C, (c) 400 °C, (d) 500 °C, and (e) 600 °C.

atmosphere form around forest dislocations since long-range diffusion of solutes from the matrix to forest and temporarily arrested mobile dislocations requires longer time. However, for concentrated substitutional alloys such as MEAs and HEAs, considering the fact that every constituent element in these alloys can serve as solute atoms and they are already abundant around forest and temporarily arrested mobile dislocations, the conventional drain mechanism becomes much less effective.

For a more detailed consideration, let us calculate the possibility that substitutional solutes catch up moving dislocations by simple lattice diffusion in the CoCrFeMnNi alloy. Using the diffusion data for the CoCrFeMnNi alloy (Tsai et al., 2013), the diffusion coefficients of composing elements can be obtained for selected temperatures of RT, 300, 400, 500, and 600 °C, as listed in Table 1, by employing the following equation:

$$D = D_0 \exp(-Q/RT) \tag{1}$$

where  $D_0$  values for Cr, Mn, Fe, Co, and Ni are 5.59, 5.01, 15.1, 9.26, and  $19.7 \times 10^{-4} \,\text{m}^2/\text{s}$ , respectively; Q values for Cr, Mn, Fe, Co, and Ni are 292.9, 288.4, 309.6, 306.9, and 317.5 kJ mol $^{-1}$ , respectively.

Based on the coefficients in Table 1, the diffusion time,  $t_{il}$ , required for an atom, i, to diffuse by a Burgers vector through the lattice can be calculated as the inverse of the average jumping rate,  $\Gamma_{il}$ , for the atom to jump from its site. Moreover,  $\Gamma_{il}$  can be related to the

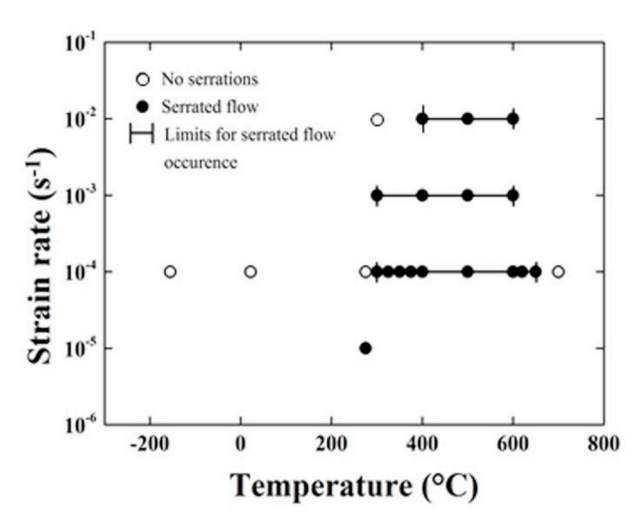


Fig. 5. The summary of the PLC effect in the CoCrFeMnNi alloy.

Table 1
Diffusion coefficients (in m<sup>2</sup>/s) of composing elements at various temperatures in the CoCrFeMnNi alloy, as calculated by Eq. (1).

	Co	Cr	Fe	Mn	Ni
RT	$9.5 \times 10^{-57}$	$6.2 \times 10^{-62}$	$9.0 \times 10^{-57}$	$2.8 \times 10^{-52}$	$9.1 \times 10^{-57}$
300 °C	$9.6 \times 10^{-32}$	$1.4 \times 10^{-33}$	$1.1 \times 10^{-31}$	$1.0 \times 10^{-29}$	$8.4 \times 10^{-32}$
400 °C	$1.2 \times 10^{-27}$	$6.0 \times 10^{-29}$	$1.4 \times 10^{-27}$	$4.9 \times 10^{-26}$	$1.0 \times 10^{-27}$
500 °C	$1.2 \times 10^{-24}$	$1.6 \times 10^{-25}$	$1.5 \times 10^{-24}$	$2.6 \times 10^{-23}$	$1.1 \times 10^{-24}$
600 °C	$2.6 \times 10^{-22}$	$7.1 \times 10^{-23}$	$3.3 \times 10^{-22}$	$3.3 \times 10^{-21}$	$2.2 \times 10^{-22}$

diffusion coefficient,  $D_{ib}$ , by the equation shown as follows (Porter and Easterling, 1981; Shewmon, 1963):

$$D_{ij} = (T_{ij} b^2) / 6$$
 (2)

Hence, the diffusion time,  $t_{il}$ , required for an atom i to diffuse by a Burgers vector through the lattice at RT, 300, 400, 500, and 600 °C can be obtained, as listed in Table 2.

On the other hand, for calculating the time required for a mobile dislocation to advance for a Burgers vector in the FCC lattice of the CoCrFeMnNi alloy, we can use the Orowan equation for tensile deformation (Reed-Hill and Abbaschian, 1992). The Orowan equation relates the strain rate  $d\varepsilon/dt$  at the tensile strain  $\varepsilon$  to the dislocation average velocity  $\nu$ , the Burgers vector b, and the dislocation density  $\rho$  (the factor 1/2 is an approximate Schmid factor between tensile strain and shear strain  $\gamma$  in polycrystalline materials):

$$d\varepsilon/dt = (1/2)d\gamma/dt = \rho bv/2 \tag{3}$$

Consider the data at RT, then the lattice constant of this alloy is  $a = 3.59 \,\text{Å}$  (Bhattacharjee et al., 2014), and the Burgers vector is  $b = 2.54 \,\text{Å}$ . For a dislocation density of  $\rho = 10^9/\text{cm}^2$  at a certain plastic strain (Gay et al., 1953), the dislocation velocity can be calculated to be  $7.9 \times 10^{-6}$  cm/s for the strain rate of  $10^{-4}/\text{s}$  at RT. This estimation of the dislocation velocity could be also valid for the condition without the dynamic recovery and recrystallization. Conversely, the dislocation velocity would be higher with the dynamic recovery and recrystallization, since the dislocation density could not be increased effectively. As the CoCrFeMnNi alloy has the recrystallization temperature of 700 °C (Bhattacharjee et al., 2014; Gay et al., 1953), we can expect the dislocation density to range from  $10^8/\text{cm}^2$  for  $600 \,\text{°C}$  (dynamic recrystallization) to  $5 \times 10^8/\text{cm}^2$  (dynamic recovery) for  $300 \,\text{°C}$  at the same plastic strain

Table 2

The time (in seconds) required for an atom to diffuse for a Burgers vector in the lattice at various temperatures in the CoCrFeMnNi alloy as calculated by Eq. (2).

	Co	Cr	Fe	Mn	Ni
RT	$1.1 \times 10^{36}$	$1.7 \times 10^{41}$	$1.2 \times 10^{36}$	$3.8 \times 10^{31}$	$1.2 \times 10^{36}$
300 °C	$1.1\times10^{11}$	$7.6 \times 10^{12}$	$9.7 \times 10^{10}$	$1.1 \times 10^{9}$	$1.3 \times 10^{11}$
400 °C	$9.2 \times 10^{6}$	$1.8 \times 10^{8}$	$7.8 \times 10^{6}$	$2.2 \times 10^{5}$	$1.1 \times 10^{7}$
500 °C	$8.7 \times 10^{3}$	$6.6 \times 10^{4}$	$7.2 \times 10^{3}$	$4.1 \times 10^{2}$	$1.0 \times 10^{4}$
600°C	40.4	1500	32.8	3.2	47.6

mentioned above. Therefore, the dislocation velocity can be calculated to be about  $7.9 \times 10^{-5}$ – $1.58 \times 10^{-5}$  cm/s if the Burgers vector, 2.54 Å, is assumed to be unchanged. As a result, the time for a mobile dislocation to advance by a Burgers vector is between  $3.2 \times 10^{-4}$  and  $1.6 \times 10^{-3}$  s at 300–600 °C. Comparing to Table 2, which lists the diffusion time for the distance of a Burgers vector, it is obvious that the diffusion time of atoms is too long to catch up and pin down dislocations in the range of 300–600 °C. Thus, this explanation based on long-range diffusion cannot account for the PLC effect.

Although moving dislocations could be obstructed by intersecting other dislocations or slowed down by passing the strong repulsion or attraction from other dislocations and have a "waiting time" for solute atoms' coming, the waiting time is still very far below that for the long-range solute diffusion in the lattice. Van den Brink et al. (van den Brink et al., 1975) estimated the average waiting time by investigating the effect of strain-rate changes on the flow stress of Au–Cu alloys in the region of strains prior to the start of serrated yielding and found that the average waiting time is from around 5 s (at the strain of 0.005) to about 40 s (at the strain of 0.05) on Au-0.5–14 wt% Cu substitutional solid solutions at the strain rate of  $4.165 \times 10^{-5}$ /s. By using the same calculation formula (van den Brink et al., 1975), we can calculate the waiting time,  $t_w$ , in the present CoCrFeMnNi alloy:

$$t_{w} = \alpha \rho b l \dot{\epsilon} = l / v = 1 / \sqrt{\rho} \cdot v \tag{4}$$

where  $\alpha$  is the same orientation factor in the Orowan equation, which is 1/2,  $\rho$  is the dislocation density, b is the Burgers vector, l is the distance between dislocations (obstacles),  $\dot{\varepsilon}$  is the strain rate, and v is the average velocity of dislocations. As the dislocation density  $\rho$  ranges from  $10^8/\text{cm}^2$  for  $600\,^\circ\text{C}$  to  $5\times10^8/\text{cm}^2$  for  $300\,^\circ\text{C}$  and dislocation velocity is about  $7.9\times10^{-5}-1.58\times10^{-5}\,\text{cm/s}$  at the strain rate of  $10^{-4}/\text{s}$  as mentioned above, the calculated waiting time ranges from  $1.1\,\text{s}$  to  $12.7\,\text{s}$ . As a result, even if waiting time is taken into consideration, there is still no enough time for solute atoms to diffuse and pin mobile dislocations by the lattice-diffusion route.

#### 4.3. New mechanism for the PLC effect in present MEAs and HEAs

To explain the PLC effect observed in the present alloy series, a mechanism of in-situ pinning with solute atoms by local diffusion in dislocation cores is proposed and demonstrated. Because there is a strain field around a solute, resulting from the atomic-size difference in the alloy system, it is expected that a higher concentration of substitutional solutes would give a greater density of lattice sites with the localized strain. For the CoNi alloy, a Co atom will have six neighboring Ni elements in the random state. Similarly, a Co in CoFeNi would have 8 different neighboring elements by  $12 \times (2/3) = 8$ ; a Co in CoCrFeNi would have 9 by  $12 \times (3/4) = 9$ ; and a Co in CoCrFeMnNi would have 9.6 by  $12 \times (4/5) = 9.6$ . Thus, more sources of the atomic-size difference in the lattice are created as the number of composing elements increases, and a dislocation is therefore exposed to abundantly surrounding compressive and tensile strain sources. It is well known that interactions exist between solutes and dislocations. To lower the overall energy, solute atoms always tend to diffuse to dislocations and cause segregation or atmosphere due to strain-relief and chemical bonding effect. As a result, considering the quinary alloy, larger atoms, such as Cr (r = 1.28 Å) and Fe (r = 1.27 Å) (Kittel, 1996), would tend to segregate to the lower part in or near edge dislocations' cores whereas Co (r = 1.25 Å) and Ni (r = 1.25 Å) to the upper part in or near edge dislocations' cores. As for the medium-sized Mn (r = 1.26 Å), they might show less strong tendency to segregate by this driving force. In addition to this, chemical bonding is an accompanying factor which affects the overall energy in segregation. Thus, this factor might also determine the actual segregation or atmosphere for achieving the lowest overall energy.

In the present model, we believe that the high diffusion rate along any direction in dislocation cores at suitable temperatures causes the fast pinning by forming the segregation or atmosphere with the abundant solute atoms, i.e., abundantly surrounding compressive and tensile strain sources, in the whole-solute matrices of MEAs and HEAs. This mechanism is very possible, if we consider the diffusion of solute atoms in dislocation cores. First, to estimate the diffusion coefficient, we use the ratio of the diffusion coefficient "in the dislocation core" to the diffusion coefficient "in the crystal lattice",  $D_p/D_l$ . Although no data of the present MEAs and HEAs are available in the literature, the diffusion data for the FCC silver obtained from the highly-cited textbook on "diffusion in solids" could be roughly applied for other FCC metals at different ratios of the experimental temperature to the melting temperature, i.e.,  $T/T_m$  (Shewmon, 1963). The data of  $D_p/D_l$  in silver are  $8 \times 10^5$  at 590 °C,  $9 \times 10^6$  at 465 °C,  $2.7 \times 10^8$  at 345 °C, and  $4.5 \times 10^{10}$  at 220 °C. Fig. 6 shows the plot of  $D_p/D_l$  versus  $T/T_m$  for silver and CoCrFeMnNi alloy. The  $D_p/D_l$  data of the CoCrFeMnNi alloy can be obtained at different experimental temperatures using the trend line of silver in Fig. 6 and the melting point of 1,607 K, which is the solidus temperature of CoCrFeMnNi alloy reported by Tsai et al. (2013). Similar to Eq. (2) for calculation of the diffusion time ( $t_{il}$ ) required for an atom i to diffuse by a Burgers vector "through the lattice", the diffusion time,  $t_{ip}$ , required for an atom i to diffuse by a Burgers vector "through the lattice", the diffusion time,  $t_{ip}$ , which relates to  $D_{ip}$ :

$$D_{ip} = (\Gamma_{ip} b^2) / 6 \tag{5}$$

Therefore, using Eq. (5), the time (in seconds) required for an atom i to diffuse for a Burgers vector "through the dislocation cores" at various temperatures in CoCrFeMnNi could be obtained as listed in Table 3. From this table, it can be understood that the time for atoms to diffuse by a Burgers vector through the dislocation core at 300 °C is comparable to the time, about from  $3.2 \times 10^{-4}$  to  $1.6 \times 10^{-3}$  s, as mentioned above, required for dislocations to advance for a Burgers vector. Moreover, at higher temperatures of 400, 500, and 600 °C, the time for atoms to diffuse in the dislocation cores are even shorter than the dislocation motion time. If we consider the waiting time, 5–40 s, at the strain rate of  $4.165 \times 10^{-5}$ /s, for mobile dislocations temporarily arrested by forest dislocations (van den Brink et al., 1975), as mentioned above, the waiting time for the strain rate of  $1 \times 10^{-2}$ /s becomes 0.021–0.17 s. It can be predicted that no PLC effect could be obtained at 300 °C, since only Mn has the sufficient rate to compete. This trend is consistent with the observation, shown in Figs. 4 and 5. On the other hand, since the waiting time for the strain rate of  $1 \times 10^{-3}$ /s

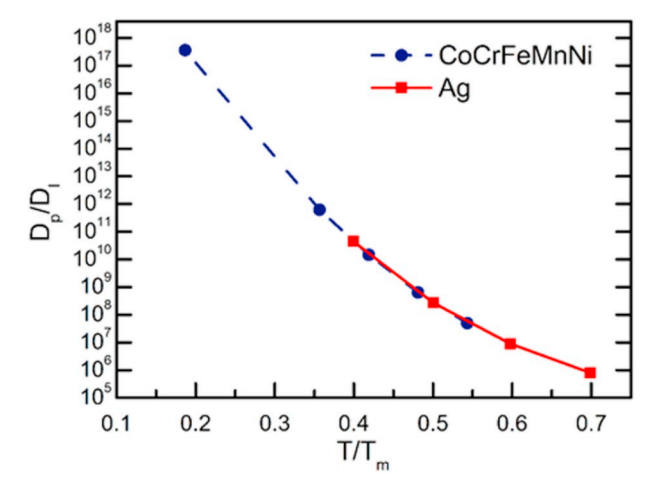


Fig. 6. The plot of D<sub>p</sub>/D<sub>1</sub> versus T/T<sub>m</sub> for silver and the estimated values for CoCrFeMnNi alloy (Shewmon, 1963).

Table 3

The time (in seconds) required for an atom to diffuse for a Burgers vector through dislocation cores at various temperatures in the CoCrFeMnNi alloy, as calculated by Eq. (5).

	Со	Cr	Fe	Mn	Ni
RT	$3.0 \times 10^{18}$	$4.7 \times 10^{23}$	$3.3 \times 10^{18}$	$1.0 \times 10^{14}$	$3.3 \times 10^{18}$
300 °C	0.18	$1.2  imes 10^{1}$	$1.6 \times 10^{-1}$	$1.8 \times 10^{-3}$	0.21
400 °C	$6.2 \times 10^{-4}$	$1.2 \times 10^{-2}$	$5.3 \times 10^{-4}$	$1.5 \times 10^{-5}$	$7.5 \times 10^{-4}$
500 °C	$1.4 \times 10^{-6}$	$1.0 \times 10^{-4}$	$1.1 \times 10^{-5}$	$6.4 \times 10^{-7}$	$1.6 \times 10^{-5}$
600 °C	$8.1 \times 10^{-7}$	$3.0 \times 10^{-5}$	$6.6 \times 10^{-7}$	$6.4 \times 10^{-8}$	$9.5 \times 10^{-7}$

becomes 0.21–1.7 s, Co, Fe, Mn, and Ni have the sufficient rate to compete with moving dislocations, and thus account for the existence of the PLC effect at 300 °C. Based on these consistencies, we can conclude the validity of the present mechanism.

As mentioned above, the actual dislocation motion during plastic deformation would encounter obstacles, such as forest dislocations. There are waiting times for these dislocations to overcome the obstacles by the aid of the thermal activation and increased stress. This activity apparently helps the solute atoms pin dislocations by the local in-situ rearrangement under the fast diffusion in mobile dislocation cores within the waiting time. Fig. 7 schematically shows different stages of atomic configurations for pinning during the dislocation motion by the proposed mechanism. The figure is plotted for simplicity by assuming that the lattice is a simple cubic structure although the present lattice is FCC, and the dislocations could be partial dislocations, which are prevalent in the quinary alloys due to the very low stacking fault energy (Carroll et al., 2015; van den Beukel, 1975). Fig. 7(a) shows an edge dislocation, which is just encountering an obstacle, Fig. 7(b) shows the in-situ rearrangement of solute atoms in the core to lower the strain-energy level and pin the dislocation, and Fig. 7(c) shows the dislocation at the new position after released from the atmosphere and then overcoming the obstacle under an increased stress.

Therefore, the mechanism behind the PLC effect is that nearby atoms along the dislocation line adjust their relative positions to lower the overall strain energy, thereby pin the dislocation. Once a dislocation is pinned, a larger force is required to break the dislocation free from the solute-atom cloud. When the released dislocation moves, it evolves into more mobile dislocation movements, and a stress drop is observed. It should be mentioned that there are many dislocation movements during plastic deformation. Different dislocations have their own encounters, and their own pinning forces developed. So, at any instant, except for those sessile dislocations, there exist both mobile dislocations moving in their slip planes and immobile dislocations pinned by solute atoms after encountering obstacles or other dislocations. Together with the increased strain and dislocation density due to dislocation multiplication, the frequency of encountering obstacles becomes higher, and the waiting time during which a dislocation trying to overcome all obstacles also increases. All these features make the microscopic deformation heterogeneous, as reflected by the wide range of differing details observed for different serrations in the same flow curve in Fig. 4.

Obviously, the in-situ local arrangement needs the local dislocation-core diffusion of the atoms to lead to successful pinning. If the temperature and diffusion rate are low, the degree of in-situ pinning would be low, and no PLC effect occurs. On the other hand, if the dislocation and thermal energy are too high, the pinning effect is destroyed. Thus, there is a suitable range for such pinning to be effective, as well as an optimal pinning effect at a certain temperature. A schematic diagram on this proposed mechanism for the PLC effect in the CoCrFeMnNi alloy is illustrated in Fig. 8. The ability of solute atoms to anchor a mobile dislocation via in-situ pinning at different temperatures in the CoCrFeMnNi samples is explained with thermal-vibration severity. This temperature effect also holds for CoFeNi and CoCrFeNi alloys.

Using the above proposed mechanism, four phenomena are observed in consistency and thus for a strong support:

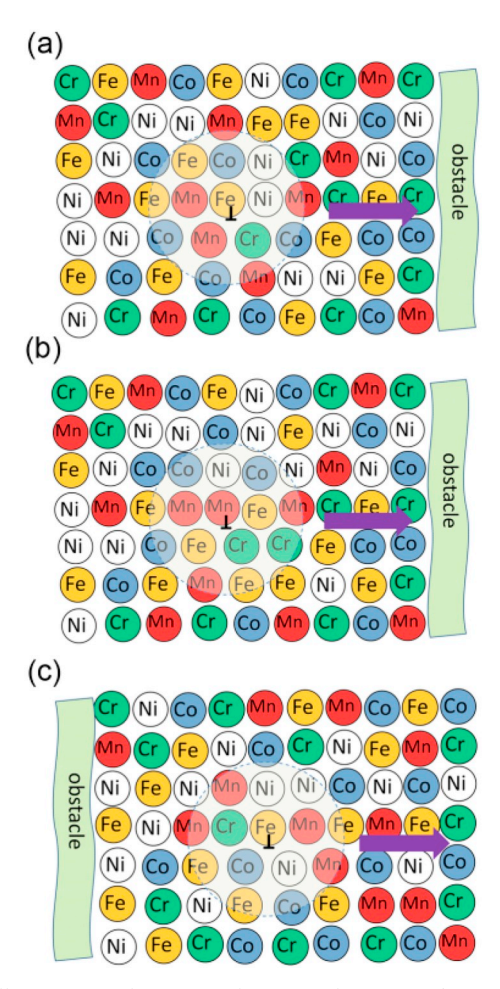


Fig. 7. The schematic diagram showing different stages of atomic configurations for pinning during the dislocation motion by the proposed mechanism in the CoCrFeMnNi alloy, in which the solute atoms in the dashed circle represent the dislocation core: (a) the dislocation, which just encounters an obstacle; (b) the in-situ rearrangement of solute atoms in the core to lower the strain-energy level and pin the dislocation; and (c) the new position of the dislocation after releasing from the atmosphere and then overcoming the obstacle under an increased stress.

- (1) Greater temperatures establish a greater probability of overcoming the energy barrier to successfully rearrange the atoms and lock the mobile dislocations. But, a limiting temperature is reached when the thermal vibration of atoms is too large to settle down the effective locking. The experiments exhibit that the working temperature range to find serration behavior at a strain rate of 10<sup>-4</sup>/s ranges is from around 300 °C–620 °C for the present quinary alloy. At the temperatures of 650 °C, no serrations are observed prior to the critical failure.
- (2) Increasing the number of solute atoms to increase the abundance and the atomic-size difference to increase the pinning force in the lattice will cause a lower and wider temperature range for the serration characteristics. This trend explains why the quinary alloy has the greatest temperature range for serrations, while the ternary alloy possesses the narrowest range. The pure metal Ni and CoNi alloy lack sufficient solute atoms and size difference, and accordingly, demonstrate no PLC effect.
- (3) A lower strain rate could lessen the temperature limit of serration features because a lower strain rate allows atoms to have more time to catch and successfully lock the dislocations. Fig. 4 demonstrates this trend. A strain rate of  $1 \times 10^{-5}$ /s produces serration characteristics at 275 °C whereas a strain rate of  $1 \times 10^{-4}$ /s does not, as seen in Fig. 4(a).
- (4) The PLC effect of CoCrFeMnNi remains when greater strain rates up to  $1 \times 10^{-2}$ /s are applied at temperatures higher than 300 °C [see in Fig. 4(c) and (d), and 4(e)]. This trend suggests that the pinning of dislocations in this alloy is fast.

In addition to conventional mechanism of PLC effect, the proposed mechanism of in-situ pinning dislocations by the local dislocation-core diffusion in dislocation cores could also be applied as a partial mechanism to explain the PLC effect observed in traditional substitutional alloys, such as the Al–Mg alloy and 316L stainless steels. That means, the proposed mechanism could have a certain contribution to the PLC effect of certain traditional substitutional alloys. The only difference is that the solute concentration is low in conventional alloys with the PLC effect, whereas the solutes in MEAs and HEAs are prevailing in the lattice. As a result, the latter alloys more effectively induce the PLC effect based on the solute contents, since they have more resources to pin dislocations. In

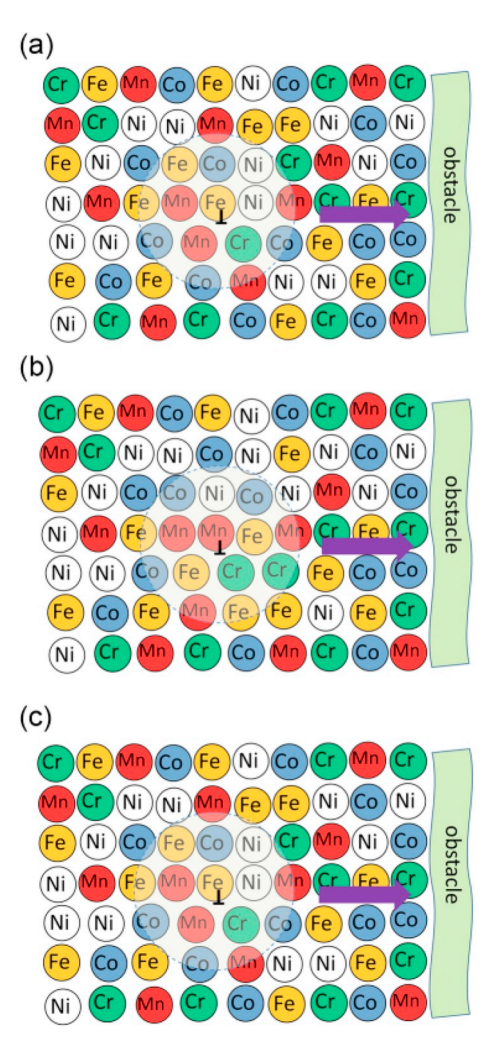


Fig. 8. Diagram explaining the ability of solute atoms to anchor a mobile dislocation via in-situ pinning at different temperatures in the CoCrFeMnNi alloy: (a) at room temperature, insufficient local dislocation-core diffusion rate does not allow the atoms to pin the dislocation by occupying low-energy positions around the dislocation; (b) at medium temperatures, sufficient local dislocation-core diffusion rate allows the atoms to pin the dislocation by occupying low-energy positions around the dislocation; and (c) At too high temperatures, the atoms vibrate too much to lock a dislocation by occupying low-energy positions around the dislocation.

addition, the atomic-size difference is very important for the proposed PLC effect, since a larger atomic-size difference could create larger pinning forces for dislocations. This is why the present equiatomic CoNi alloy having very small atomic-size differences does not display the PLC effect. This is also why Al-Mg alloys with the large atomic-size difference could display the effect (Cottrell, 1953; Matsuura et al., 1969) although they have lower Mg concentrations. Ma et al. reported the important two factors affecting the solution hardening: solubility enthalpy per solute and volumetric mismatch (Ma et al., 2013). They concluded that (1) the solubility enthalpy per solute is related to the volumetric mismatch by a power law; (2) the strengthening potential of high volumetric mismatch solutes is severely limited by their low solubility; and (3) for each annealing temperature, there exists an optimal solute-volume mismatch to achieve maximum strength. Based on our mechanism in which high solubility can provide more abundant solutes in pinning arrested dislocations and larger atomic difference can provide stronger interaction in pinning arrested dislocations, it is expected that solubility and atomic size difference have a trade-off to obtain pronounced PLC effect.

#### 5. Conclusions

The effects of varying temperatures and strain rate on the PLC effect during tensile testing on alloys ranging from FCC-LEAs to FCC-HEAs have been investigated to reveal the relevant mechanism. The conclusions are drawn as follows:

(1) The PLC effect is found in a specific temperature range and strain rates for MEAs and HEAs only, in which the quinary CoCrFeMnNi alloy displays the PLC effect in the widest temperature range from 300 °C to 620 °C and at greater strain rates up to

- $1 \times 10^{-2}$ /s except at the temperature of 300 °C.
- (2) The pinning of dislocations by solute atoms is fast enough to result in the PLC effect even at high strain rate in MEAs and HEAs. Through qualitative and quantitative deduction, the traditional mechanisms were disproved and a new mechanism of in-situ dislocations pinning by the local dislocation-core diffusion of solutes in dislocation cores was proposed and verified.
- (3) The local dislocation-core diffusion model is ideal for the PLC effect in concentrated alloys like MEAs and HEAs in the 300 °C–620 °C temperature range, because solute atoms in or near the dislocation cores are able to make in-situ rearrangement and pin dislocations in a very short time period. Instead of taking the long-range diffusion route for solute atoms to move through the lattice or forest dislocation cores and catch moving or impeded dislocations, the proposed mechanism requires only the local rearrangement of the solute atoms around cores of impeded dislocations.
- (4) The effects of the number of elements, temperature, and strain rate on the serration behavior have been successfully explained based on this proposed new mechanism. The interaction between substitutional solute atoms and dislocations, the kinetics to the low-energy configuration, and their effects on plastic behavior are clarified for the present concentrated alloys, such as MEAs and HEAs.
- (5) The mechanism of in-situ pinning dislocations by the local dislocation-core diffusion in dislocation cores could be applied as a partial mechanism to explain the PLC effect observed in traditional substitutional alloys, such as the Al-Mg alloy and 316 stainless steels.
- (6) Based on the proposed mechanism in which high solubility can provide more abundant solutes for pinning arrested dislocations and larger atomic-size difference can provide stronger interaction in pinning arrested dislocations, it is expected that solubility and atomic-size difference have a trade-off to obtain pronounced PLC effect.

#### **Declarations of interest**

None

#### Acknowledgments

The present work was supported by the Ministry of Science and Technology (Taiwan) grant numbers MOST 106-2218-E-007-019. The support provided by the High-Entropy Materials Center from the Featured Areas Research Center Program within the framework of the Higher Education Sprout Project by the Ministry of Education in Taiwan is greatly appreciated. We also thank John Weber, Greg Schwarz, and Abid Khan for helpful conversations. We gratefully acknowledge the support of the US National Science Foundation (NSF) through grants DMR 100520, DMS 1069224 (KAD), DMR-1611180 and 1809640 (PKL), the Department of Energy (DOE), NEUP 00119262, DE-FE-0008855 (PKL) with Drs. Hess, Curry, Cooper, Farlkas, Shiflet, Cedro, Jensen, Tan, and Lesica as contract monitors. KAD and PKL thank DOE for the support through the project, DE-FE-0011194, with the project manager, Dr. Mullen. PKL very much appreciates the support of the U.S. Army Research Office project (W911NF-13-1-0438) with the program managers, Drs. Bakas, Mathaudhu, and Stepp.

#### References

Antonaglia, J., Xie, X., Tang, Z., Tsai, C.W., Qiao, J.W., Zhang, Y., Laktionova, M.O., Tabachnikova, E.D., Yeh, J.W., Senkov, O.N., Gao, M.C., Uhl, J.T., Liaw, P.K., Dahmen, K.A., 2014. Temperature effects on deformation and serration behavior of high entropy alloys (HEAs). J. Occup. Med. 66, 2002–2008. https://doi.org/10.1007/s11837-014-1130-9.

Bhattacharjee, P.P., Sathiaraj, G.D., Zaid, M., Gatti, J.R., Lee, C., Tsai, C.W., Yeh, J.W., 2014. Microstructure and texture evolution during annealing of equiatomic CoCrFeMnNi high-entropy alloy. J. Alloy. Comp. 587, 544–552. https://doi.org/10.1016/j.jallcom.2013.10.237.

Buffington, F.S., Hirano, K., Cohen, M., 1961. Self diffusion in iron. Acta Metall. 9, 434–439. https://doi.org/10.1016/0001-6160(61)90137-7.

Cantor, B., Chang, I.T.H., Knight, P., Vincent, A.J.B., 2004. Microstructural development in equiatomic multicomponent alloys. Mater. Sci. Eng. A - Struct. Mater. 375, 213–218. https://doi.org/10.1016/j.msea.2003.10.257.

Carroll, R., Lee, C., Tsai, C.W., Yeh, J.W., Antonaglia, J., Brinkman, B.A., LeBlanc, M., Xie, X., Chen, S., Liaw, P.K., Dahmen, K.A., 2015. Experiments and model for serration statistics in low-entropy, medium-entropy, and high-entropy alloys. Sci. Rep. 5, 16997. https://doi.org/10.1038/srep16997.

Chuang, M.H., Tsai, M.H., Wang, W.R., Lin, S.J., Yeh, J.W., 2011. Microstructure and wear behavior of Al<sub>x</sub>Co<sub>1.5</sub>CrFeNi<sub>1.5</sub>Ti<sub>y</sub> high-entropy alloys. Acta Mater. 59, 6308–6317. https://doi.org/10.1016/j.actamat.2011.06.041.

Cottrell, A.H., 1953. A note on the Portevin-Le Chatelier effect. Phil. Mag. 44, 829-832. https://doi.org/10.1080/14786440808520347.

Cottrell, A.H., Jaswon, M.A., 1949. Distribution of solute atoms round a slow dislocation. Proc. Roy. Soc. Lond. Math. Phys. Sci. 199, 104–114. https://doi.org/10.1098/rspa.1949.0128.

Dieter, G.E., 1988. Mechanical Metallurgy, SI, metric ed. McGraw-Hill London, New York.

Fu, J.X., Cao, C.M., Tong, W., Hao, Y.X., Peng, L.M., 2017. The tensile properties and serrated flow behavior of a thermomechanically treated CoCrFeNiMn high-entropy alloy. Mat. Sci. Eng. A - Struct. 690, 418–426. https://doi.org/10.1016/j.msea.2017.03.031.

Gay, P., Hirsch, P.B., Kelly, A., 1953. The estimation of dislocation densities in metals from X-ray data. Acta Metall. 1, 315–319. https://doi.org/10.1016/0001-6160(53)90106-0.

Halim, H., Wilkinson, D.S., Niewczas, M., 2007. The Portevin-Le Chatelier (PLC) effect and shear band formation in an AA5754 alloy. Acta Mater. 55, 4151–4160. https://doi.org/10.1016/j.actamat.2007.03.007.

Hector, L.G., Zavattieri, P.D., 2011. Nucleation and propagation of Portevin-Le Châtelier bands in austenitic steel with twinning induced plasticity. Experimental and Applied Mechanics ume 6. Springer, New York, pp. 855–863. https://doi.org/10.1007/978-1-4419-9792-0\_118.

Hemphill, M.A., Yuan, T., Wang, G.Y., Yeh, J.W., Tsai, C.W., Chuang, A., Liaw, P.K., 2012. Fatigue behavior of Al<sub>0.5</sub>CoCrCuFeNi high entropy alloys. Acta Mater. 60, 5723–5734. https://doi.org/10.1016/j.actamat.2012.06.046.

Hong, S.G., Lee, S., 2005. Mechanism of dynamic strain aging and characterization of its effect on the low-cycle fatigue behavior in type 316L stainless steel. J. Nucl. Mater. 340, 307–314. https://doi.org/10.1016/j.jnucmat.2004.12.012.

Kittel, C., 1996. Introduction to Solid State Physics, seventh ed. Wiley, New York.

- Kok, S., Bharathi, M.S., Beaudoin, A.J., Fressengeas, C., Ananthakrishna, G., Kubin, L.P., Lebyodkin, M., 2003. Spatial coupling in jerky flow using polycrystal plasticity. Acta Mater. 51, 3651–3662. https://doi.org/10.1016/S1359-6454(03)00114-9.
- Lebyodkin, M.A., Kobelev, N.P., Bougherira, Y., Entemeyer, D., Fressengas, C., Gornakov, V.S., Lebedkina, T.A., Shashkov, I.V., 2012. On the similarity of plastic flow processes during smooth and jerky flow: statistical analysis. Acta Mater. 60, 3729–3740. https://doi.org/10.1016/j.actamat.2012.03.026.
- Li, Z., Pradeep, K.G., Deng, Y., Raabe, D., Tasan, C.C., 2016. Metastable high-entropy dual-phase alloys overcome the strength–ductility trade-off. Nature 534, 227–230. https://doi.org/10.1038/nature17981.
- Ma, D., Friak, M., von Pezold, J., Raabe, D., Neugebauer, J., 2013. Ab initio identified design principles of solid-solution strengthening in Al. Sci. Technol. Adv. Mater. 14, 025001. https://doi.org/10.1088/1468-6996/14/2/025001.
- Matsuura, K., Nishiyam, T., Koda, S., 1969. Portevin-Le Chatelier effect in aluminum-magnesium alloys. Trans. Jpn. Inst. Met. 10, 429–436. No DOI available. Website: https://www.jim.or.jp/journal/e/10/06/429.html.
- McCormic, Pg, 1973. Portevin-Le Chatelier effect in a pressurized low-carbon steel. Acta Metall. 21, 873–878. https://doi.org/10.1016/0001-6160(73)90144-2. Min, J., Hector, L.G., Zhang, L., Sun, L., Carsley, J.E., Lin, J., 2016. Plastic instability at elevated temperatures in a TRIP-assisted steel. Mater. Des. 95, 370–386. https://doi.org/10.1016/j.matdes.2016.01.113.
- Miracle, D.B., Senkov, O.N., 2017. A critical review of high entropy alloys and related concepts. Acta Mater. 122, 448–511. https://doi.org/10.1016/j.actamat.2016.
- Mulford, R.A., Kocks, U.F., 1979. New observations on the mechanisms of dynamic strain aging and of jerky flow. Acta Metall. 27, 1125–1134. https://doi.org/10. 1016/0001-6160(79)90130-5.
- Otto, F., Dlouhy, A., Somsen, C., Bei, H., Eggeler, G., George, E.P., 2013. The influences of temperature and microstructure on the tensile properties of a CoCrFeMnNi high-entropy alloy. Acta Mater. 61, 5743–5755. https://doi.org/10.1016/j.actamat.2013.06.018.
- Pink, E., Kumar, S., 1995. Patterns of serrated flow in a low-carbon steel. Mater. Sci. Eng. A Struct. Mater. 201, 58-64. https://doi.org/10.1016/0921-5093(95) 09772-4.
- Porter, D.A., Easterling, K.E., 1981. Phase Transformations in Metals and Alloys. Van Nostrand Reinhold, New York.
- Reed-Hill, R.E., Abbaschian, R., 1992. Physical Metallurgy Principles, third ed. PWS-Kent Pub., Boston.
- Rizzi, E., Hahner, P., 2004. On the Portevin-Le Chatelier effect: theoretical modeling and numerical results. Int. J. Plast. 20, 121–165. https://doi.org/10.1016/S0749-6419(03)00035-4.
- Rodriguez, P., 1984. Serrated plastic flow. Bull. Mater. Sci. 6, 653-663. https://doi.org/10.1007/BF02743993.
- Senkov, O.N., Wilks, G.B., Miracle, D.B., Chuang, C.P., Liaw, P.K., 2010. Refractory high-entropy alloys. Intermetallics 18, 1758–1765. https://doi.org/10.1016/j.intermet.2010.05.014.
- Shewmon, P.G., 1963. Diffusion in Solids. McGraw-Hill, New York.
- Sleeswyk, A.W., 1958. Slow strain-hardening of ingot iron. Acta Metall. 6, 598-603. https://doi.org/10.1016/0001-6160(58)90101-9.
- Tang, Z., Yuan, T., Tsai, C.W., Yeh, J.W., Lundin, C.D., Liaw, P.K., 2015. Fatigue behavior of a wrought Al<sub>0.5</sub>CoCrCuFeNi two-phase high-entropy alloy. Acta Mater. 99, 247–258. https://doi.org/10.1016/j.actamat.2015.07.004.
- Tong, C.J., Chen, M.R., Chen, S.K., Yeh, J.W., Shun, T.T., Lin, S.J., Chang, S.Y., 2005. Mechanical performance of the Al<sub>x</sub>CoCrCuFeNi high-entropy alloy system with multiprincipal elements. Metall. Mater. Trans. A 36A, 1263–1271. https://doi.org/10.1007/s11661-005-0218-9.
- Tsai, K.Y., Tsai, M.H., Yeh, J.W., 2013. Sluggish diffusion in Co-Cr-Fe-Mn-Ni high-entropy alloys. Acta Mater. 61, 4887–4897. https://doi.org/10.1016/j.actamat. 2013.04.058.
- van den Beukel, A., 1975. Theory of the effect of dynamic strain aging on mechanical properties. Phys. Status Solidi 30, 197–206. https://doi.org/10.1002/pssa. 2210300120.
- van den Brink, S.H., van den Beukel, A., McCormick, P.G., 1975. Strain rate sensitivity and the portevin-le chatelier effect in Au–Cu alloys. Phys. Status Solidi 30, 469–477. https://doi.org/10.1002/pssa.2210300205.
- Wang, W.Y., Shang, S.L., Wang, Y., Han, F., Darling, K.A., Wu, Y., Xie, X., Senkov, O.N., Li, J., Hui, X.D., 2017. Atomic and electronic basis for the serrations of refractory high-entropy alloys. npj Comput. Mater. 3, 23. https://doi.org/10.1038/s41524-017-0024-0.
- Xiang, G.F., Zhang, Q.C., Liu, H.W., Jiang, H.F., Wu, X.P., 2006. Deformation measurements of three types of Portevin-Le Chatelier bands. Chin. Phys. 15, 2378–2384. No DOI available. Website: https://iopscience.iop.org/article/10.1088/1009-1963/15/10/032.
- Yeh, J.W., 2006. Recent progress in high-entropy alloys. Ann. Chim.-Sci. Mat. 31, 633–648.
- Yeh, J.W., 2013. Alloy design strategies and future trends in high-entropy alloys. J. Occup. Med. 65, 1759-1771. https://doi.org/10.1007/s11837-013-0761-6.
- Yeh, J.W., Chen, S.K., Lin, S.J., Gan, J.Y., Chin, T.S., Shun, T.T., Tsau, C.H., Chang, S.Y., 2004. Nanostructured high-entropy alloys with multiple principal elements: novel alloy design concepts and outcomes. Adv. Eng. Mater. 6, 299–303. https://doi.org/10.1002/adem.200300567.
- Yeh, J.W., Chen, Y.L., Lin, S.J., Chen, S.K., 2007. High-entropy alloys a new era of exploitation. Mater. Sci. Forum 560, 1–9. https://doi.org/10.4028/www.scientific.net/MSF.560.1.
- Yilmaz, A., 2011. The Portevin-Le Chatelier effect: a review of experimental findings. Sci. Technol. Adv. Mater. 12, 063001. https://doi.org/10.1088/1468-6996/12/6/063001.
- Youssef, K.M., Zaddach, A.J., Niu, C.N., Irving, D.L., Koch, C.C., 2015. A novel low-density, high-hardness, high-entropy alloy with close-packed single-phase nanocrystalline structures. Mater. Res. Lett. 3, 95–99. https://doi.org/10.1080/21663831.2014.985855.
- Zavattieri, P., Savic, V., Hector Jr., L., Fekete, J., Tong, W., Xuan, Y., 2009. Spatio-temporal characteristics of the Portevin–Le Châtelier effect in austenitic steel with twinning induced plasticity. Int. J. Plast. 25, 2298–2330. https://doi.org/10.1016/j.ijplas.2009.02.008.
- Zhang, Y., Liu, J.P., Chen, S.Y., Xie, X., Liaw, P.K., Dahmen, K.A., Qiao, J.W., Wang, Y.L., 2017. Serration and noise behaviors in materials. Prog. Mater. Sci. 90, 358–460. https://doi.org/10.1016/j.pmatsci.2017.06.004.
- Zhang, Y., Qiao, J.W., Liaw, P.K., 2016. A brief review of high entropy alloys and serration behavior and flow units. J. Iron Steel Res. Int. 23, 2–6. https://doi.org/10.1016/S1006-706X(16)30002-4.
- Zhang, Y., Zuo, T., Cheng, Y., Liaw, P.K., 2013. High-entropy alloys with high saturation magnetization, electrical resistivity, and malleability. Sci. Rep. 3, 1455. https://doi.org/10.1038/srep01455.
- Zhang, Y., Zuo, T.T., Tang, Z., Gao, M.C., Dahmen, K.A., Liaw, P.K., Lu, Z.P., 2014. Microstructures and properties of high-entropy alloys. Prog. Mater. Sci. 61, 1–93. https://doi.org/10.1016/j.pmatsci.2013.10.001.